Geodesy and Geodynamics 8 (2017) 260–272

Contents lists available at ScienceDirect

Geodesy and Geodynamics

journal homepages: www.keaipublishing.com/en/journals/geog;
http://www.jgg09.com/jweb_ddcl_en/EN/volumn/home.shtml

A GOCE only gravity model GOSG01S and the validation of GOCE related satellite gravity models

Xinyu Xu [a, b, *], Yongqi Zhao [a], Tilo Reubelt [c], Robert Tenzer [a]

[a] School of Geodesy and Geomatics, Wuhan University, 129 Luoyu Road, Wuhan 430079, China
[b] Key Laboratory of Geospace Environment and Geodesy, Ministry of Education, 129 Luoyu Road, Wuhan 430079, China
[c] Institute of Geodesy, University of Stuttgart, Geschwister-Scholl-Str. 24D, 70174 Stuttgart, Germany

ARTICLE INFO

Article history:
Received 11 January 2017
Accepted 1 March 2017
Available online 23 April 2017

Keywords:
Earth's gravity field
Geopotential model
Gravity gradient
Validation
Satellite-to-satellite tracking

ABSTRACT

We compile the GOCE-only satellite model GOSG01S complete to spherical harmonic degree of 220 using Satellite Gravity Gradiometry (SGG) data and the Satellite-to-Satellite Tracking (SST) observations along the GOCE orbit based on applying a least-squares analysis. The diagonal components (V_{xx}, V_{yy}, V_{zz}) of the gravitational gradient tensor are used to form the system of observation equations with the band-pass ARMA filter. The point-wise acceleration observations (a_x, a_y, a_z) along the orbit are used to form the system of observation equations up to the maximum spherical harmonic degree/order 130. The analysis of spectral accuracy characteristics of the newly derived gravitational model GOSG01S and the existing models GOTIM04S, GODIR04S, GOSPW04S and JYY_GOCE02S based on their comparison with the ultra-high degree model EIGEN-6C2 reveals a significant consistency at the spectral window approximately between 80 and 190 due to the same period SGG data used to compile these models. The GOCE related satellite gravity models GOSG01S, GOTIM05S, GODIR05S, GOTIM04S, GODIR04S, GOSPW04S, JYY_GOCE02S, EIGEN-6C2 and EGM2008 are also validated by using GPS-leveling data in China and USA. According to the truncation at degree 200, the statistic results show that all GGMs have very similar differences at GPS-leveling points in USA, and all GOCE related gravity models have better performance than EGM2008 in China. This suggests that all these models provide much more information on the gravity field than EGM2008 in areas with low terrestrial gravity coverage. And STDs of height anomaly differences in China for the selected truncation degrees show that GOCE has improved the accuracy of the global models beyond degree 90 and the accuracies of the models improve from 24 cm to 16 cm. STDs of geoid height differences in USA show that GOSG01S model has best consistency comparing with GPS-leveling data for the frequency band of the degree between 20 and 160.

1. Introduction

The Gravity field and steady-state Ocean Circulation Explorer (GOCE) satellite mission was launched in March 2009 and started its operational phase in September 2009. One of the principal scientific objectives of this satellite mission was to recover the global gravity field with an expected accuracy of about 1–2 cm (in terms of geoid) or 1 mGal (in terms of gravity) at the level of a spectral resolution of about degree 200 in terms of spherical harmonics, which corresponds to about 100 km at the equator [1–3]. GOCE was the first satellite mission to measure gravitational gradients directly using a high-precision electrostatic gravity gradiometer by the differential acceleration technique [4], which was used to recover the medium-to-higher frequency signal of the gravitational field. The on-board GPS receiver provides the Satellite-to-Satellite Tracking (SST) data, which were used to determine the precise kinematic (PKI) orbit with a cm-level accuracy [5], and consequently to recover the long-wavelength part of the gravity field. Therefore,

* Corresponding author. School of Geodesy and Geomatics, Wuhan University, 129 Luoyu Road, Wuhan 430079, China. Fax: +86 027 68778371.
E-mail address: xyxu@sgg.whu.edu.cn (X. Xu).
Peer review under responsibility of Institute of Seismology, China Earthquake Administration.

Production and Hosting by Elsevier on behalf of KeAi

http://dx.doi.org/10.1016/j.geog.2017.03.013

the full-frequency, high-precision GOCE satellite gravitational model could be estimated by combining the SST and SGG data [1].

Generally, there are several different numerical techniques applied to recover the global gravitational model (GGM) by processing the GOCE SGG observables. Probably the most commonly used techniques are: the direct approach (DIR), the time-wise approach (TIM), and the space-wise approach (SPW) corresponding to three types of models which are determined by the GOCE High Level Processing Facility (HPF) [6]. Until now, the fifth-generation models derived using the TIM [7] and DIR [8] approaches, and the fourth-generation model derived by the SPW approach have been released by the European Space Agency (http://icgem.gfz-potsdam.de/ICGEM). Considering the SGG data period used in modeling GOSG01S, the fourth-generation models, GO_CONS_GCF_2_TIM_R4 [6,9–12], GO_CONS_GCF_2_DIR_R4 [13–16] and GO_CONS_GCF_2_SPW_R4 [17–19], are preferably used for comparison with other recently released GOCE related models. In this study we denote these models as GOTIM04S, GODIR04S and GOSPW04S respectively. A brief description (such as modeling approach, data processing strategies, input data, maximum degree and order, etc.) about the models are given in Table 1.

Moreover, there are also other GOCE related satellite gravity models which were developed using different data processing strategies, such as the GOCO-S model series (http://www.goco.eu), ITG-Goce02 [20], JYY_GOCE02S/04S [21] and DGM-1S [22]. The latest model of GOCO-S model series was GOCO05S released [23]. In this study, JYY_GOCE02S are preferably used for the validation of our model, because they were computed using nearly the same data period as for the fourth-generation TIM and DIR solutions, although we also given the validation of other models. The brief information about GOCO03S, JYY_GOCE02S, ITG-Goce02 and DGM-1S are also given in Table 1.

In addition to these SGG processing strategies, the tensor invariant method for the GOCE gravity recovery was developed and applied [24–26]. The semi-analytical (SA) method was investigated in detail [27,28], and applied to real GOCE data [29].

All the above summarized GGMs derived using SST data of GOCE mission processed using different strategies, such as the energy integration approach [30], the average acceleration approach [31], the short-arc integral approach [11], and the celestial mechanics approach [32]. All these SST analysis methods including the point-wise acceleration approach [33] for the determination of the long-wavelength gravitational spectrum based on processing the GOCE SST data were compared and analyzed [34]. They demonstrated that, except for the energy integration approach, all these methods provide similar results. We will show similar results from the GOCE related models comparison.

In this study, we apply a newly designed method to process the GOCE data. According to this method, the point-wise acceleration approach is used for the first time for the combination with SGG data in order to derive a full GOCE-only gravity field model. Then, the (eight-order) band-pass ARMA filter with the pass-band of 5–41 mHz is applied to process the diagonal components of the gravitational gradient tensor (GGT), which is different with that used for the determination of GOTIM04S and GOSPW04S. Furthermore, we apply the second-order Tikhonov regularization technique (TRT) only to the near-zonal coefficients in order to decrease the influence with the increasing order for a particular degree of spherical harmonics, which is different with that used for the determination of GOTIM04S, GOSPW04S and JYY_GOCE02S. We also apply the General Cross Validation (GCV) technique to estimate the optimal regularization parameters, which is not used in other methods. And the variance factors of the observations (V_{xx}, V_{yy}, V_{zz}) for every independent continuous arc are estimated by applying the Variance Component Estimation (VCE) technique. In analogy with processing of GOTIM04S and GOSPW04S, we do not use any reference model in order to obtain a GOCE-only solution. The content of the manuscript is organized into 5 Sections, beginning with the descriptions of the functional and stochastic models in Section 2. The applied processing strategies are summarized in Section 3. The results are presented and validated in Section 4. Summary and concluding remarks are given in Section 5.

2. Functional and stochastic models

In this section we provide a brief overview of the functional and stochastic models which include a least-squares (LS) approach with colored noise filtering for processing the SGG data and the point-wise acceleration approach for processing the SST data.

2.1. Functional model for SGG

In order to process the SGG observations along the GOCE satellite orbit, the LS approach is applied here. The Earth's gravitational potential V at a point (r, θ, λ) is defined [35].

$$V(r,\theta,\lambda) = \frac{GM}{a}\sum_{n=0}^{N_{\max}}\sum_{m=0}^{n}\left(\frac{a}{r}\right)^{n+1}\left(\overline{C}_{nm}\cos m\lambda + \overline{S}_{nm}\sin m\lambda\right)\overline{P}_{nm}(\cos\theta) \tag{1}$$

where GM is the geocentric gravitational constant, a is the semi-major axis of the reference ellipsoid, $\overline{P}_{nm}$ are the (fully-normalized) associated Legendre functions of degree n and order m, $\overline{C}_{nm}$ and $\overline{S}_{nm}$ the (fully-normalized) geopotential coefficients which describe the external gravitational field of the Earth, and $N_{\max}$ is the maximum degree of the harmonic expansion. The 3-D position is defined in the Earth's Fixed Reference Frame (EFRF) by the spherical coordinates (r, θ, λ), where r is the geocentric radius, θ and λ are the spherical co-latitude and longitude respectively.

We further define the gravitational potential V in Eq. (1) by means of the Fourier series expansion [36]. Then we can write

$$\begin{aligned} V(r,\theta,\lambda) &= \sum_{m=0}^{\infty}\left[A_m^V(r,\theta)\cos m\lambda + B_m^V(r,\theta)\sin m\lambda\right] \\ \left.\begin{matrix}A_m^V(r,\theta)\\ B_m^V(r,\theta)\end{matrix}\right\} &= \sum_{n=m}^{\infty} H_{nm}^V(r,\theta)\left\{\begin{matrix}\overline{C}_{nm}\\ \overline{S}_{nm}\end{matrix}\right., \\ H_{nm}^V(r,\theta) &= \lambda_n\overline{P}_{nm}(\cos\theta), \lambda_n = \frac{GM}{a}\left(\frac{a}{r}\right)^{n+1} \end{aligned} \tag{2}$$

where $A_m^V(r,\theta), B_m^V(r,\theta)$ are the Fourier coefficients, and $H_{nm}^V(r,\theta)$ are the conversion coefficients between $A_m^V(r,\theta), B_m^V(r,\theta)$ and $\overline{C}_{nm}, \overline{S}_{nm}$. It should be noted that we can use Eq. (2) to express the gravitational potential for a single point (r, θ, λ) because Eq. (2) is just the transformation of Eq. (1) by interchanging the summation over n and m. So, $A_m^V(r,\theta), B_m^V(r,\theta)$ are not constants any more for the observations along the GOCE orbit.

From Eqs. (1) and (2), the components V_{ij} of the second-order (Marussi) gravitational gradient tensor (GGT) are defined in the Local North-Oriented Frame (LNOF) as follows

$$\begin{aligned} V_{ij}(r,\theta,\lambda) &= \sum_{m=0}^{\infty}\left[A_m^{ij}(r,\theta)\cos m\lambda + B_m^{ij}(r,\theta)\sin m\lambda\right], \\ \left.\begin{matrix}A_m^{ij}(r,\theta)\\ B_m^{ij}(r,\theta)\end{matrix}\right\} &= \sum_{n=m}^{\infty} H_{nm}^{ij}(r,\theta)\left\{\begin{matrix}\overline{C}_{nm}\\ \overline{S}_{nm}\end{matrix}\right. \end{aligned} \tag{3}$$

Table 1
The brief description of several GOCE related satellite gravity field models.

Model name	d/o	Input data	Data processing strategies	Regularization/Prior information	Statistical model for SGG/Weight
GOTIM05S	280	**GOCE only** SGG: V_{xx}, V_{yy}, V_{zz}, V_{xz} (Nov.2009–Oct.2013) SST: PKI orbits	SGG: time-wise method, 280 d/o SST: short-arc integral method, 150 d/o LS: strictly inverse	Kaula regularization: (near-) zonal coefficients and high-degree coefficients (201–280 d/o)	Digital ARMA filters as whitening filters
GODIR05S	300	**Combination** SGG: V_{xx}, V_{yy}, V_{zz}, V_{xz} (Nov.2009–Oct.2012) SST: GRACE (10 years), LAGEOS (25 years)	SGG: direct solution method, 300 d/o SST: dynamic method (solving orbits and potential coefficients together), 130 d/o LS: strictly inverse	Kaula regularization: high-degree coefficients (180–300 d/o) And spherical cap regularization with the iteration computation	A filter with a pass band of 8.3–125.0 mHz
GOTIM04S	250	**GOCE only** SGG: V_{xx}, V_{yy}, V_{zz}, V_{xz} (Nov.2009–Jun.2012) SST: PKI orbits	SGG: time-wise method, 250 d/o SST: short-arc integral method, 130 d/o LS: strictly inverse	Kaula regularization: (near-) zonal coefficients and high-degree coefficients (180–250 d/o)	Full de-correlation with ARMA filter
GODIR04S	260	**Combination** SGG: V_{xx}, V_{yy}, V_{zz}, V_{xz} (Nov.2009–Jul.2012) SST: GRACE (10 years), LAGEOS (25 years)	SGG: direct solution method, 260 d/o SST: dynamic method (solving orbits and potential coefficients together), 130 d/o LS: strictly inverse	Kaula regularization: high-degree coefficients (200–260 d/o) And spherical cap regularization with the iteration computation	8.3–125.0 mHz band-pass filter
GOSPW04S	280	**GOCE only** SGG: V_{xx}, V_{yy}, V_{zz}, V_{xz} (Nov.2009–Jul.2012) SST: PKI orbits	SGG: space-wise method, 280 d/o SST : energy balance method, 150 d/o Spherical harmonic analysis	Regularization matrix estimated by signal covariance model from EIGEN-6C3stat	Wiener filter and whitening filter
JYY_GOCE02S	230	**Combination** SGG: V_{xx}, V_{yy}, V_{zz}, V_{xz} (Nov.2009–Aug.2012) SST: GOCE PKI orbits Polar gap data: geoid from ITG-GRACE2010s	SGG: direct solution method, 230 d/o SST: short-arc integral method, 120 d/o LS: strictly inverse	Pseudo-observations from ITG-GRACE2010s for polar gap stabilization	IIR (butterworth) filter with the pass band 5–100 mHz
GOCO03S	250	**Combination** SGG: (V_{xx}, V_{yy}, V_{zz}, V_{xz} (Nov.2009–Apr.2011) SST: GRACE (7 years, ITG-Grace2010s), CHAMP(8 years), SLR(5 years)	SGG: time-wise method, 250 d/o SST: short-arc integral method, 160 d/o LS: strictly inverse	Kaula regularization: high-degree coefficients (180–250 d/o)	Full de-correlation with ARMA filter
ITG-Goce02	240	**GOCE only** SGG: V_{xx}, V_{yy}, V_{zz} (Nov.2009–Jun.2010) SST: PKI orbits (7.5 months)	SGG: direct solution method based on short arcs, 240 d/o SST: short-arc integral method, 130 d/o LS: strictly inverse	Kaula regularization: the coefficients (5–240 d/o)	Full variance-covariance matrix from the observation residuals referred to a reference model
DGM-1S	250	**Combination** SGG: V_{xx}, V_{yy}, V_{zz} (Nov.2009–Dec.2010) SST: GRACE KBR(7 years), GOCE PKI orbits (14 months)	SGG: direct solution method, 250 d/o SST: average acceleration method, 130 d/o LS: pre-conditioned conjugate gradients	Kaula regularization: high-degree coefficients (180–250 d/o) And using empirically defined 7-parameter high-pass filter	Frequency-dependent data weighting based on PSDs of the observation residuals referred to the prior model or the iteration solution

where the indexes i and j define the gravitational gradient components (xx, yy, zz, xy,…) with respect to the LNOF axes (x, y, z). For more detailed definitions of the coefficients $A_m^{ij}(r,\theta), B_m^{ij}(r,\theta)$ and $H_{nm}^{ij}(r,\theta)$, we refer to the reference [36]. The expression in Eq. (3) defines observation equations for the SGG components in the LNOF coordinate frame.

As seen in Eq. (3), the observations V_{ij} should be in the LNOF. But the observed GGT components (V_{xx}, V_{yy}, V_{zz}) are defined in GRF. Generally, we could transform the observations from GRF to LNOF using the following rotation matrix

$$\boldsymbol{R}_{\mathrm{G}}^{\mathrm{L}} = \boldsymbol{R}_{\mathrm{G}}^{\mathrm{I}} \boldsymbol{R}_{\mathrm{I}}^{\mathrm{E}} \boldsymbol{R}_{\mathrm{E}}^{\mathrm{L}} \tag{4}$$

where $\boldsymbol{R}_{\mathrm{G}}^{\mathrm{I}}$ is the transformation matrix from GRF to IRF (which can be computed by the quaternions from the EGG_IAQ_2 data), $\boldsymbol{R}_{\mathrm{I}}^{\mathrm{E}}$ is the transformation matrix from IRF to EFRF (which can be computed from the SST_PRM_2 data), and $\boldsymbol{R}_{\mathrm{E}}^{\mathrm{L}}$ is the transformation matrix from EFRF to LNOF (which can be computed using satellite orbits). In this case, however, the high-precision components (V_{xx}, V_{yy}, V_{zz}) will be contaminated by the transformation, because of the presence of the colored noise in the observations and a relatively low accuracy of the components (V_{xy}, V_{yz}). This method is thus not suitable to recover the gravity field [37]. Therefore, we transformed the base functions instead of transforming the GGT observations in Eq. (3). This is done by applying the matrix $\boldsymbol{R}_{\mathrm{G}}^{\mathrm{I}}$ and its transposed matrix in the observation equation (see Eq. (3)). Hence, we have

$$\boldsymbol{V}^{\mathrm{GRF}} = \boldsymbol{R}_{\mathrm{G}}^{\mathrm{L}} \boldsymbol{V}^{\mathrm{LNOF}} \boldsymbol{R}_{\mathrm{L}}^{\mathrm{G}} \tag{5}$$

where $\boldsymbol{V}^{\mathrm{GRF}}$ and $\boldsymbol{V}^{\mathrm{LNOF}}$ represent the gravitational gradient tensor in GRF and LNOF respectively.

2.2. Functional model for SST

The point-wise acceleration approach for gravity field determination from kinematic orbits was originally introduced by Reubelt [33] and for the first time applied successfully to real data from the CHAMP mission [38–40]. Later on, the performance of the

point-wise acceleration approach was demonstrated for GOCE-SST long-wavelength recovery [34,41,42] as well as for long-wavelength temporal gravity recovery from CHAMP-SST [43].

Considering the inertial coordinate reference frame, from the second Newton's law

$$\mathbf{F} = m\boldsymbol{a} \tag{6}$$

We can express the equation of satellite motion by its acceleration at time t as follows

$$\ddot{\boldsymbol{r}}(t) = \boldsymbol{a}(t) \tag{7}$$

where $\ddot{\boldsymbol{r}}(t)$ is the second-order derivative of the satellite position $\boldsymbol{r}(t)$, and $\boldsymbol{a}(t)$ is the total acceleration of the satellite caused by all types of forces acting on the satellite, which in principle, includes the Earth's gravitational acceleration $\boldsymbol{a}_{\mathrm{g}}(t)$ and additional disturbing accelerations. The latter comprises third-body accelerations $\boldsymbol{a}_{\mathrm{b}}(t)$, tidal accelerations $\boldsymbol{a}_{\mathrm{t}}(t)$, relativistic effects $\boldsymbol{a}_{\mathrm{r}}(t)$, variations in gravitation $\boldsymbol{a}_{\mathrm{f}}(t)$ caused by short-term fluctuations (atmosphere, oceans, hydrology, etc.), and non-gravitational accelerations $\boldsymbol{a}_{\mathrm{n}}(t)$ due to atmospheric drag and solar radiation [41].

The Earth's gravitational acceleration $\boldsymbol{a}_{\mathrm{g}}(t)$ cannot directly be computed based on applying the gradient operator ∇ to the geopotential function $V(t)$ in EFRF. Instead, the conversion between the Inertial Reference Frame (IRF) and LNOF has to be taken into consideration in the definition of the equation of satellite motion. A more detailed description of these reference frames can be found in the product data handbook [44]. The observation equation of the acceleration approach is then given by

$$\begin{aligned}\mathbf{R}(t)\left\{\ddot{\boldsymbol{r}}(t) - \boldsymbol{a}_{\mathrm{b}}(t) - \boldsymbol{a}_{\mathrm{t}}(t) - \boldsymbol{a}_{\mathrm{r}}(t) - \boldsymbol{a}_{\mathrm{n}}(t) - \boldsymbol{a}_{\mathrm{f}}(t)\right\} \\ = \begin{pmatrix} a_x \\ a_y \\ a_z \end{pmatrix} = \nabla V(t) = \begin{pmatrix} \dfrac{\partial V(t)}{\partial x} \\ \dfrac{\partial V(t)}{\partial y} \\ \dfrac{\partial V(t)}{\partial z} \end{pmatrix}\end{aligned} \tag{8}$$

where $\boldsymbol{R}(t)$ is the transformation matrix between IRF to LNOF at time t. The transformation from IRF to LNOF could be realized in two steps by applying the conversion from IRF to EFRF, followed by a conversion to LNOF.

As seen in Eq. (8), the system of observation equations for processing the SST data is formed for three acceleration components along the satellite orbit in the LNOF. The gravitational disturbing accelerations $\boldsymbol{a}_{\mathrm{b}}(t)$, $\boldsymbol{a}_{\mathrm{t}}(t)$, $\boldsymbol{a}_{\mathrm{r}}(t)$ and $\boldsymbol{a}_{\mathrm{f}}(t)$ are computed using existing models [41], while the non-gravitational accelerations $\boldsymbol{a}_{\mathrm{n}}(t)$ are measured with the GOCE on-board accelerometers and compensated by the drag-free system.

2.3. LS combination of SST and SGG

For the linear observations defined in Eqs. (3) and (8), the functional and statistical models of the gravitational field recovery from the SGG and SST data are defined by a standard Gauss-Markov model. It reads

$$\mathbf{y} = \boldsymbol{A}\boldsymbol{x} + \boldsymbol{\varepsilon}, \quad E\{\boldsymbol{y}\} = \boldsymbol{A}\boldsymbol{x}, \quad D\{\boldsymbol{y}\} = \sigma_0^2\boldsymbol{Q} = \sigma_0^2\boldsymbol{P}^{-1} \tag{9}$$

where $\boldsymbol{y}$ is the vector of observations, $\boldsymbol{A}$ is the design matrix, $\boldsymbol{x}$ is the vector of (unknown) geopotential parameters to be estimated, $\boldsymbol{\varepsilon}$ is the vector of observation errors, $D\{\boldsymbol{y}\}$ is the error variance-covariance matrix, $\boldsymbol{P}$ is the weight matrix, $\boldsymbol{Q}$ is the inverse of the weight matrix, and σ_0^2 is the variance component.

In our case, the observation vector $\boldsymbol{y}$ comprises the diagonal components (V_{xx}, V_{yy}, V_{zz}) of GGT in the gradiometer reference frame (GRF) and three components (a_x, a_y, a_z) of the Earth's gravitational accelerations in GRF. It should be noted that the V_{xz} component can be profitably used for gravity field recovery, such as the time-wise approach [9] and the space-wise approach [19]. We denote these observations (V_{xx}, V_{yy}, V_{zz}, a_x, a_y, a_z) in the observation vector by indexing them as $\boldsymbol{y}_i$ (i = 1,2,3,4,5,6). The same notation is applied to the design and weight matrices, i.e., $\boldsymbol{A}_i$ and $\boldsymbol{P}_i$. From Eq. (9), the geopotential parameters $\boldsymbol{x}$ can be estimated by applying the VCE technique as follows [45].

$$\widehat{\boldsymbol{x}} = \boldsymbol{N}^{-1}\boldsymbol{W} \tag{10}$$

where the normal matrix and vector reads

$$\boldsymbol{N} = \sum_{i=1}^{6}\left(\frac{1}{\sigma_i^2}\boldsymbol{A}_i^T\boldsymbol{P}_i\boldsymbol{A}_i\right), \quad \boldsymbol{W} = \sum_{i=1}^{6}\left(\frac{1}{\sigma_i^2}\boldsymbol{A}_i^T\boldsymbol{P}_i\boldsymbol{y}_i\right) \tag{11}$$

and σ_i^2 are the variance factors of observations $\boldsymbol{y}_i$. By applying Helmert's method [46], the variance factors σ_i^2 can be computed iteratively according to

$$\widehat{\sigma}_i^2 = (\boldsymbol{A}_i\widehat{\mathbf{x}} - \boldsymbol{y}_i)^T\boldsymbol{P}_i(\boldsymbol{A}_i\widehat{\boldsymbol{x}} - \boldsymbol{y}_i) \Big/ \left(l_i - tr\left(\frac{1}{\sigma_i^2}\boldsymbol{A}_i^T\boldsymbol{P}_i\boldsymbol{A}_i\boldsymbol{N}^{-1}\right)\right) \tag{12}$$

where l_i is the number of observations $\boldsymbol{y}_i$.

Actually, the observations could form the independent arcs for every component (V_{xx}, V_{yy}, V_{zz}, a_x, a_y, a_z). Hence, it should be more convenient to estimate the variance factors for independent arcs (such as 1 month data period), because of consideration of the data precision differences in different time epochs. In this study, the variance factors for every independent arc of the SGG data V_{xx}, V_{yy}, V_{zz} are estimated using this strategy, although this strategy will increase processing time.

Due to the GOCE data gap in polar areas, the least-squares solution is ill-posed. To stabilize the solution, we applied Tikhonov's regularization technique [47]. The regularization matrix $\boldsymbol{K}$ and the regularization parameter α were then applied in Eq. (11) as follows [48].

$$\boldsymbol{N} = \sum_{i=1}^{6}\left(\frac{1}{\sigma_i^2}\boldsymbol{A}_i^{\mathrm{T}}\boldsymbol{P}_i\boldsymbol{A}_i\right) + \alpha\boldsymbol{K}, \quad \boldsymbol{W} = \sum_{i=1}^{6}\left(\frac{1}{\sigma_i^2}\boldsymbol{A}_i^{\mathrm{T}}\boldsymbol{P}_i\boldsymbol{y}_i\right) \tag{13}$$

Here we used the second-order Tikhonov regularization matrix [49] of which the diagonal elements are defined as follows

$$k_{jj} = n_j^2(n_j + 1)^2 \tag{14}$$

where n_j is the degree of the geopotential coefficient related to a row number j. The second-order Tikhonov regularization matrix with the regularization parameter $\alpha = 10^{10}$ is very close to the Kaula regularization matrix, which uses the inverse of Kaula's rule [50].

$$k_{jj} = n_j^4 \tag{15}$$

The regularization parameter α is estimated by applying the GCV technique. It reads [48,49].

$$\alpha_{\mathrm{gcv}} = \arg\min \frac{n\|\boldsymbol{y} - \boldsymbol{A}\boldsymbol{x}\|^2}{\left(n - tr\left(\boldsymbol{A}(\boldsymbol{A}^{\mathrm{T}}\boldsymbol{P}\boldsymbol{A} + \alpha\boldsymbol{K})^{-1}\boldsymbol{A}^{\mathrm{T}}\boldsymbol{P}\right)\right)^2} \tag{16}$$

where n is the number of the observations.

3. Data processing

In order to estimate the final GOCE based gravity field model, all SGG and SST data products released by ESA are needed to be pre-processed. And the normal equations corresponding to the SST and SGG observations are formed independently. To deal with the colored noise in SGG observations, the band-pass filtering could be used to suppress the large noise outside the MBW. So the high-precision long-wavelength gravity field could not be recovered by using the SGG data, which mainly contribute to the median-to-short wavelengths of the gravity field. The high-precision full-band GOCE only gravity filed model could be estimated by combing SST and SGG observations. And the regularization technique should be applied to solve the ill-posed problem caused by the polar data gaps. In the following sub-sections, the detailed processing procedures of the SST and SGG observations are described.

3.1. Data description

The released gravitational gradient product EGG_NOM_2 and the precise science orbits SST_PSO_2 were used to determine the GOCE-only model GOSG01S. Note that these data products can be accessed at: http://eo-virtual-archive1.esa.int/Index.html. These data products also include several sub-products for gravity field recovery, namely the EGG_NOM_2 product mainly includes gravity gradient tensor observations GGT in GRF, the attitude quaternions EGG_IAQ_2 used for the transformation from IRF to GRF, and the common-mode accelerations EGG_CCD_2C. The SST_PSO_2 product includes the kinematic orbits SST_PKI_2, the variance-covariance information SST_PCV_2 of the precise PKI orbits, reduced-dynamic orbits SST_PRD_2, and the quaternions SST_PRM_2 used for the transformation from EFRF to IRF.

The data period of the EGG_NOM_2 product used for forming the SGG observation equations is from 1st of November, 2009 until 31st of May, 2012. We selected only the high-precision diagonal components (V_{xx}, V_{yy}, V_{zz}) of GGT. The data period of SST_PKI_2 and SST_PCV_2 products used to form the SST observation equations is from 1st of November, 2009 until 5th of July, 2010 (R2-period). Due to the increasing magnetic activity for the years 2011 and 2012 the quality of the GOCE SST solutions is reduced [51] and severe structures emerge in the SST-only solutions. Thus we think it is appropriate to use only the SST data of the R2-period for the combination with SGG for our GOCE model.

3.2. Data preprocessing

To select appropriate data of a good quality, we preprocessed the initial data by applying outlier detection, interpolation, and unification of the time for the different observations. Moreover, the application of the ARMA filter for the SGG observation equation requires that the datasets are continuous for every independent arc.

3.2.1. Preprocessing for SGG data

For the original continuous SGG observations, data records with the flag 4 were deleted. This obviously introduced data gaps. Hence, to obtain a continuous data set, the observations at these data gaps were estimated by applying the 7-point Lagrange polynomial interpolation when the length of the data gap was less than 40s. Otherwise, the data were split into independent arcs. When forming the SGG observation equations, the SST_PRD_2 product with 10 s sampling was used to interpolate the 1s sampling orbits according to the time of SGG data, again using the 7-point Lagrange polynomial interpolation. The corresponding SST_PRM_2 observations were then interpolated according to the time of SGG data using the method described in Ref. [44]. After gross outlier elimination, data gaps interpolation and data splitting, we obtained in total 44 independently continuous SGG arcs and about 20.5 months of the validated SGG data.

The power spectral density (PSD) of the diagonal components (V_{xx}, V_{yy}, V_{zz}) and the trace of GOCE GGT are shown in Fig. 1, which are estimated by the 71 days data from 1st of November, 2009 to 10th of January, 2010. We note that the trace of GOCE GGT represents the total error of the components V_{xx}, V_{yy} and V_{zz}. The PSD curve of the trace shows that a high-precision signal in the SGG observations is achieved only within the measurement bandwidth (MBW) from 5 to 100 mHz, while the noise outside of this interval has characteristics of a colored noise, especially for the $1/f$ behavior at low frequencies, which is consistent with the design requirements [37]. The colored noise behavior refers to the fact that the SGG observations are auto-correlated in time. Consequently, the error variance-covariance matrix is a fully-occupied matrix, which is hard to deal with directly due to limited computational capacity currently available. A possible method of processing the colored noise in SGG data is to apply a whitening filtering technique to both sides of the linear observation equation [52]. The filter model corresponds to the PSD of the colored noise. This procedure is equivalent to the application of the full error variance-covariance matrix estimated by the PSD of the filter-frequency response [52]. Here we apply the band-pass ARMA filter instead of the whitening filter, which is defined as [53].

$$x(n) + \sum_{i=1}^{p} a_i x(n-i) = \sum_{i=0}^{q} b_i w(n-i) \tag{17}$$

where (a_i, b_i) are coefficients of the filter, p the order of the auto-regressive part, q the order of the moving average part, $x(n)$ the output discrete time series, and $w(n)$ the input time series to be filtered. The corresponding frequency response $H(z)$ is defined as

$$H(z) = \frac{\sum_{i=0}^{q} b_i z^{-i}}{1 + \sum_{i=1}^{p} a_i z^{-i}} \tag{18}$$

3.2.2. Preprocessing for SST data

For the SST data, we used the accelerations computed from the a priori gravitational model EGM96 [54] to detect the gross outliers. The outlier threshold was set equal to 4000 mGal. Based on this criterion, less than 0.01% data were classified as gross errors and subsequently removed from data set. The selections of both, the reference model and threshold, were chosen to be very

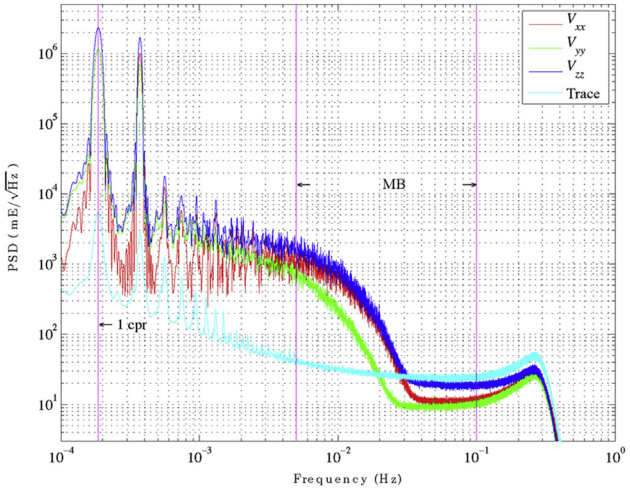

Fig. 1. PSDs of the diagonal components (V_{xx}, V_{yy}, V_{zz}) and the trace of GOCE GGT.

conservative in order to make sure that the selected observations are independent to the applied a priori gravitational model.

The numerical differentiation technique is used to derive the accelerations of satellite motion $\ddot{\boldsymbol{r}}(t)$ from the kinematic satellite positions (for GOCE mission, PKI orbits released by ESA). This is done by applying the eight-order (nine-point) differentiator [33,41]. For reducing the high-frequency noise amplification generated by the numerical differentiation technique, a simple low pass filter method could be used, such as a down-sampling procedure. In Baur et al. [41] this was established by means of an Extended Differentiation Filter (EDF) with a step width of $\Delta t = 30$ s in order to account for deficiencies of the empirically estimated covariance matrices in recording the high frequent noise. Another option for filtering the high frequency noise is a straightforward error propagation of the orbit covariance matrices to acceleration covariance matrices by means of the differentiation scheme. Using these acceleration covariance matrices directly for data-weighting (or alternatively for creating a whitening filter by means of an ARMA process, see Section 3.2.1) means an appropriate high-pass filtering. In newer GOCE-SST analysis this lead to a slightly better performance [34,42] and thus this procedure was selected in our study together with a moderate Extended Differentiation Filter (EDF5) technique with$\Delta t = 5$s [41,42].

3.3. Forming SGG observation equations

For the SGG data, we set the maximum degree and order as 220. It corresponds to 48837 geopotential coefficients to be determined. Considering tens of millions of SGG observations, forming the normal equation and inverting the normal matrix will demand huge computation resources, which could not be realized using single processors. We separated the observations into short arcs (with an average time span of about 4 h), and formed the normal equations of the diagonal components V_{xx}, V_{yy} and V_{zz} independently for every short arc by using multi-processors on the high performance computer. The final system of normal equations for every continuous arc, corresponding to the three components (V_{xx}, V_{yy}, V_{zz}), was formed by summing up all the normal equations established for the short arcs and applying a relative weight of 1. For combining the independent continuous arcs and different observations (V_{xx}, V_{yy}, V_{zz}), however, the variance factors were estimated for every independent continuous arc.

To deal with the colored noise of the observations, the (eight-order) band-pass ARMA filter ($p = q = 8$) with the pass-band between 5 and 41 mHz was applied on both sides of the observation equations formed according to Eq. (9) for all three components (V_{xx}, V_{yy}, V_{zz}) in the entire data period. The maximum value of the pass-band, 41 mHz, was computed from$f_{\max} = N_{\max}/T_r$. This corresponds to the maximum degree and order $N_{\max} = 220$ for one satellite orbital revolution $T_r = 5383$ s [55]. Because of the warming-up problem of the ARMA filter, the first 2000 samples of every arc should be abandoned, which will cause huge loss of data. To avoid this problem, we prepared the data to have 2000 record overlaps between two successive arcs in one continuous data period.

3.4. Forming SST observation equations

After the outlier detection of the kinematic orbits, the accelerations (a_x, a_y, a_z) and the weight matrix $\boldsymbol{P}$ in Eq. (9) were derived based on applying the EDF5 and error propagation according to the orbit arc length of 15 min. For every independent orbital arc, the error statistical model was computed by the straightforward error propagation from the PKI orbit variance-covariance information provided by SST_PCV_2 [42]. The non-conservative forces from the GOCE on-board accelerometers (common mode accelerations) were also included in the observation equations and a constant empirical parameter was estimated for every 10 successive arcs for each coordinate direction in the GRF. Although GOCE is kept quasi drag-free in along-track direction, it is of benefit for the very low degree gravity field coefficients [34] to account for the residual non-conservative accelerations mainly caused by the insensitivity of the accelerometers to low-frequency signal. The observation equations for independent arcs were then generated individually. The final system of normal equations of SST was solved by assembling the normal equations with initial variance factors for independent arcs. Moreover, the VCE technique was applied to estimate the variance factors of the independent arcs iteratively. The VCE was established in the orbit frame (along-track, cross-track, radial) since this is a natural system for GPS-induced kinematic orbit errors [34,56,57]. This would effectively reduce the contribution of the arcs with large residuals to the final solution, e.g., the influence of the along-track component of February 2010 which was contaminated by missing GGT observations and failing drag-free compensation. For details of the GOCE SST real data processing based on straightforward error propagation of orbit variance-covariance information we refer to the references [34,42].

3.5. SGG and SST combination, regularization

The final solution was estimated by combining the systems of normal equations formed independently for the diagonal components (V_{xx}, V_{yy}, V_{zz}) and the SST data. The most important aspect of this processing step was to choose relative weights between these observations by estimating the variance factors in Eq. (11). The variance factors for the SGG and SST data were determined independently. For the SGG data, the variance factors of 44 continuous arcs of the observations (V_{xx}, V_{yy}, V_{zz}) were estimated iteratively by applying the VCE technique [45]. For every independent continuous arc, the initial values of the variance factors were set as 3 mE (for V_{xx}, V_{yy}) and 6 mE (for V_{zz}) according to the error levels of (V_{xx}, V_{yy}, V_{zz}) from their PSDs (Fig. 1), which was consistent with the results in the Ref. [58]. After the third iteration, the variance factors of the diagonal components (V_{xx}, V_{yy}, V_{zz}) have converged to certain different values for different observation arcs. These estimated variances were then used to combine the SST data with the components V_{xx}, V_{yy} and V_{zz} in forming the final system of normal equations. Considering that nearly the same estimation strategy was used in forming the SST observation equations (in Section 3.4), the variance factor of the SST observation equations in Eq. (11) was set equal to 1 for combining the SST and SGG data. This is because the SST observations were weighted by the corresponding variance-covariance information and the estimated variance factors of the independent orbit arcs.

Since the ill-posed problem caused by the polar data gap influenced mainly the near-zonal coefficients [59], the diagonal elements k_{jj} of the regularization matrix were applied only to the coefficients with $m < m_r$ (where $m_r = 20$ is the maximum order for the regularization). Since the influence of the ill-posed problem decreases continuously with an increasing order for a certain harmonic degree, the regularization matrix elements k_{jj} should generally also decrease with an increasing order. According to this principle, the values of k_{jj} were computed from

$$k_{jj} = n_j^2 (n_j + 1)^2 (m - m_r)^2, \quad \text{for } m < m_r, m_r = 20 \tag{1}$$

4. Results and validation

Based on the data processing strategies described in Section 3, we estimated individually three solutions, namely the SST-only

gravitational model, the SGG-only gravitational model, and the combined SGG and STT gravitational model, called herein GOSG01S. The systems of normal equations were solved by means of Cholesky's decomposition. As mentioned before, these three models have been obtained without using any a priori gravitational model, disregarding even the normal gravity field.

4.1. Comparison with EIGEN-6C2

To evaluate the spectral error characteristics of our three developed models, the ultra-high degree model EIGEN-6C2 [60] was used for comparison. The combined model EIGEN-6C2 was determined from GRACE, GOCE, LAGEOS, marine and terrestrial gravity data. Note that this model is available at the GFZ website (http://icgem.gfz-potsdam.de/ICGEM). This model shows a very good agreement with global GPS-leveling data, including the GPS-leveling points in China [61]. Therefore, we selected this model for the validation of our solutions. The degree RMS of the coefficient differences between our three solutions and the EIGEN-6C2 model are shown in Fig. 2. For Fig. 2b, in order to remove the effect of the polar gap, the coefficients with the order less than $m_n = |0.5\pi - I| \times n$ (with inclination I in radians) are omitted when estimating the degree RMS [41]. As expected, the combined SGG and SST model with the regularization technique applied, GOSG01S, has a better accuracy than the SST-only and SGG-only models. The SST-only model shows better performance than the SGG-only model up to degree 35. Moreover, the large errors in Fig. 2a are mainly caused by the polar data gap. The errors could be reduced by the regularization technique. By comparing the spectra of the differences between our solutions and EIGEN-6C2 in Fig. 3, we could see that the largest differences are distributed mainly within the zonal and near-zonal coefficients ($m < 20$) as well as within the high-degree coefficients. These differences, attributed to the polar data gap, were reduced by applying the regularization. Moreover, as seen in Fig. 3, the SST-only and SGG-only models have a good quality at lower and high degrees respectively. The main

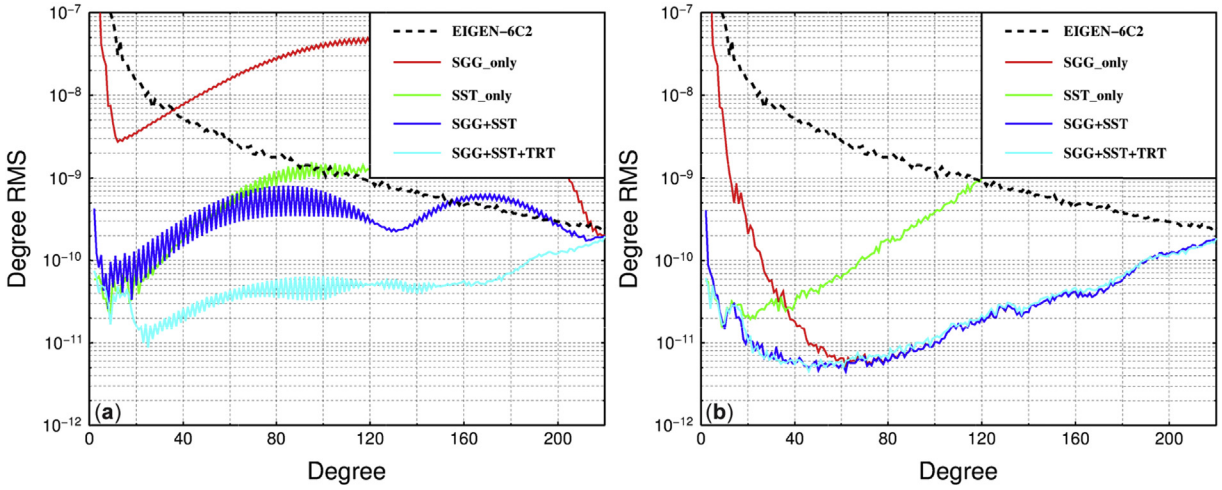

Fig. 2. Degree RMS of the coefficient differences between our solutions and EIGEN-6C2: (**a**) no orders are omitted; (**b**) orders $m < m_n$ omitted. EIGEN-6C2 signal (black dashed line), the SGG-only solution (red line), the SST-only solution (green line), the combined SGG and SST solution without the regularization (blue line), and the combined SGG and SST solution with the regularization (cyan line).

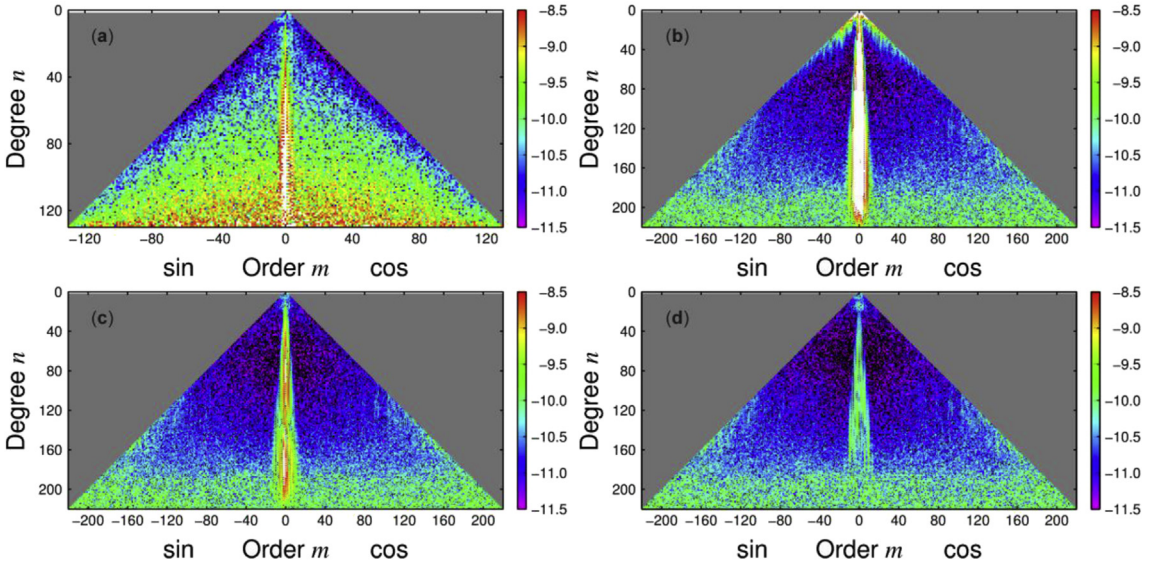

Fig. 3. Spectra of the geopotential coefficient differences between the different solutions and EIGEN-6C2: (**a**) the SST-only solution; (**b**) the SGG-only solution; (**c**) the combined SGG and SST solution before regularization; and (**d**) the combined SGG and SST solution after regularization.

contribution to the combined model from the SGG data is thus nearly above degree/order 50. As also seen from the comparison with EIGEN-6C2, the regularization significantly improved the accuracy of the final solution (GOSG01S).

We further compared the accuracy of our final model, GOSG01S, with the similar GOCE-only derived models GOTIM04S, GOSPW04S, the combination models GODIR04S and JYY_GOCE02S. The degree RMS of the coefficient differences between GOCE-related models (GOSG01S, GOTIM04S, GODIR04S, GOSPW04S and JYY_GOCE02S) and EIGEN-6C2 are plotted in Fig. 4. As seen from the figure, the GOCE-related models except GODIR04S are very close to each other at the spectral window approximately between 80 and 190 in Fig. 4b, while there are the large differences among them at the spectral window less than 160 in Fig. 4a. This means that the large differences among them mainly come from the low-order terms because of the different regularization approaches applied for dealing with the polar gap problem. As seen from these differences, the GODIR04S model has a better agreement with EIGEN-6C2 at the long-to-medium part of the gravitational spectrum than others. The main reason is that GODIR04S and EIGEN-6C2 comprise the contribution from GRACE data, and the same processing strategy of the SGG data was used for setting up the normal equation matrix. The JYY_GOCE02S model is more close to EIGEN-6C2 than GOTIM04S, GOSPW04S and GOSG01S at the spectral window approximately between 30 and 160 in Fig. 4a because pseudo-observations from ITG-GRACE2010s in polar gap area were used for the regularization in modeling the JYY_GOCE02S model. GOTIM04S more closely agrees with EIGEN-6C2 above degree 190. This finding could be partly explained by the fact that Kaula's regularization technique was applied to the GOTIM04S coefficients above degree 180, whereas we applied the regularization only to the zonal and near-zonal coefficients of the GOSG01S model. Moreover, the coefficients of the frequency band between 80 and 190 mainly contributed by the SGG data are very close to each other if we took no account of the influence of the polar gap, although the different processing strategies of SGG data are applied in modeling. Comparing with GODIR04S, other models are more close to each other in Fig. 4b, especially at the low-degree spectrum which is only contributed from the GOCE SST-hl data.

In order to analyze the GOSG01S contribution to the long-to-medium wavelengths of the gravitational field, we plotted the geoid differences between the GOCE only models (GOSG01S, GOTIM04S and GOSPW04S) and the ultra-high degree models (EGM2008 [62] and EIGEN-6C2) in Fig. 5, using the spherical harmonic expansion complete to degree/order 200. From the figure, GOSG01S, GOTIM04S and GOSPW04S models show the same pattern globally. Comparing with EGM2008 (in Fig. 5 left column), the largest differences are distributed in areas of Himalaya, Tibet, Andes, Amazonia, central Africa, and Antarctica, where terrestrial gravity data are sparse or completely absent. Consequently, the accuracy of EGM2008 in these areas is low. In contrast, the geoid differences between the GOCE only models and EGM2008 over open oceans are very small and normally distributed. This indicates that the GOCE only models have a very good reliability. By analogy with findings of the Refs. [9,21,58], we could conclude that, if considering the spatial resolution complete to degree of 200, GOSG01S provides significantly more information on the gravity field in these areas than EGM2008. The results also show that the GOSG01S, GOTIM04S and GOSPW04S models are very close to EIGEN-6C2 except the polar area.

4.2. Validation using GPS-leveling data

In this paragraph we used the GPS-leveling information in China and USA to validate the accuracy of the GOSG01S. For this purpose we used 649 GPS-leveling points in China [61] and 6169 GPS-leveling points in USA [63]. Note that GPS-leveling data in USA are available at the NGS website (http://www.ngs.noaa.gov). The accuracy of GOSG01S at these GPS-leveling points was also compared with the GOTIM05S, GODIR05S, GOTIM04S, GODIR04S, GOSPW04S, JYY_GOCE02S, GOCO03S, EIGEN-6C2 and EGM2008 models with the maximum degree and order 200. The statistics of the differences between the GGMs and GPS-leveling geoid/quasi-geoid heights in China and USA are summarized in Tables 2 and 3. These differences comprise also the GGM omission errors. As seen from this validation, the GOSG01S, GOTIM05S, GODIR05S, GOTIM04S, GODIR04S, GOSPW04S, JYY_GOCE02S, GOCO03S and EIGEN-6C2 models have nearly the same accuracy; the STD of differences of these models differ less than 6 mm. Moreover, we can see that all models compiled using GOCE data have a significantly better accuracy in China than EGM2008, while all these models (including EGM2008) have nearly the same accuracy in USA. This is explained by the fact that terrestrial gravity data in China were lower accuracy or not incorporated in processing the EGM2008 model.

The same analysis was repeated by taking into consideration the GGM omission errors. The omission errors were estimated using the EGM2008 coefficients between the spherical harmonic

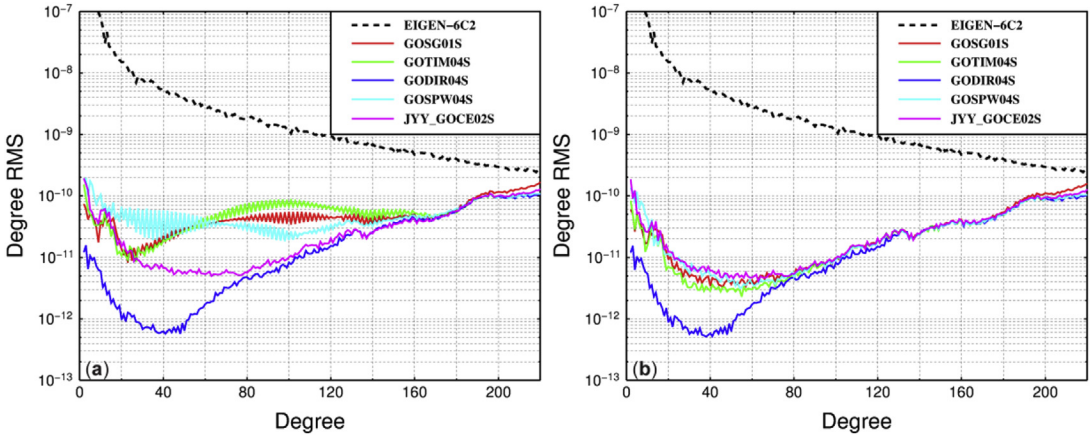

Fig. 4. Degree RMS of the coefficient differences of the GOSG01S, GOTIM04S, GODIR04S, GOSPW04S and JYY_GOCE02S models with respect to EIGEN-6C2: (**a**) no orders are omitted; (**b**) orders $m < m_n$ omitted.

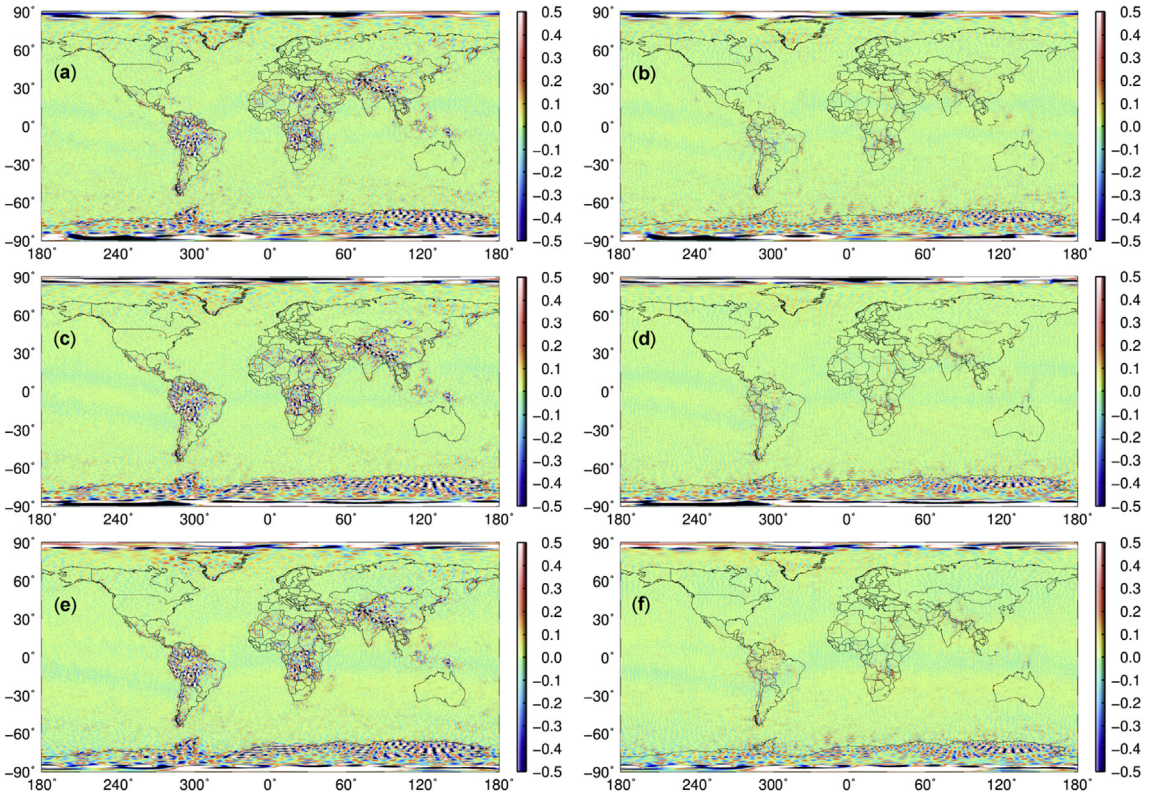

Fig. 5. Geoid differences between the GOCE only models (GOSG01S, GOTIM04S and GOSPW04S) and the ultra-high degree models (EGM2008 and EIGEN-6C2) computed using the spherical harmonic resolution up to degree of 200: (**a**) the differences between GOSG01S and EGM2008; (**b**) the differences between GOSG01S and EIGEN-6C2; (**c**) the differences between GOTIM04S and EGM2008; (**d**) the differences between GOTIM04S and EIGEN-6C2; (**e**) the differences between GOSPW04S and EGM2008; and (**f**) the differences between GOSPW04S and EIGEN-6C2. (Unit: m).

degrees from 200 up to 2190. We note that the degree and order of EIGEN-6C2 model is up to 1949. The statistics of geoid/quasi-geoid differences computed using GGMs and GPS-leveling data are given in Table 4. Similarly to the results presented in Tables 2 and 3, all GGMs compiled using GOCE data have again very similar differences at GPS-leveling points in China and USA. We also see that all investigated models (including EGM2008) have a very similar accuracy in USA, while the EGM2008 model corrected for the omission errors has again a lower accuracy in China than other models.

In order to analyze the accuracy of GOSG01S according to the different frequency corresponding to the degree of the model, we use the same approach for the validation of GOCE gravity field models in the Ref. [64]. Fig. 6 shows the STDs of height anomaly differences in China and STDs of geoid height differences in USA for the selected truncation degrees and orders in steps of 10 starting from the degree and order 10 to 220 for GOCE related models GOSG01S, GOTIM04S, GODIR04S, GOSPW04S, JYY_GOCE02S and EGM2008. The omission errors of the GOCE related models and EGM2008 up to the truncation degree are computed by EGM2008 from the truncation degree to degree 2190. So for EGM2008, the STD of height anomaly/geoid height differences in China and USA is always a constant for different degrees. In China, these GOCE related models have nearly the same accuracy for the degree less than 200. Starting from degree 200, the accuracy of GOSG01S becomes a little bit worse than other models. The STDs of the GOCE related models which decrease from 24 cm to

Table 2
Validation of the GOSG01S, GOTIM05S, GODIR05S, GOTIM04S, GODIR04S, GOSPW04S, GOCO03S, JYY_GOCE02S, EIGEN-6C2 and EGM2008 models up to degree and order 200 using GPS-leveling data in China (649 points) (unit: m). The omission errors were disregarded.

Model	Mean	Max	Min	RMS	STD
GOSG01S	0.050	3.220	−3.024	0.571	±0.569
GOTIM05S	0.048	3.232	−3.007	0.570	±0.569
GODIR05S	0.049	3.219	−3.016	0.571	±0.569
GOTIM04S	0.050	3.233	−3.033	0.571	±0.569
GODIR04S	0.047	3.216	−3.034	0.572	±0.570
GOSPW04S	0.043	3.209	−3.055	0.571	±0.570
GOCO03S	0.046	3.260	−3.049	0.573	±0.571
JYY_GOCE02S	0.055	3.228	−3.037	0.572	±0.569
EIGEN-6C2	0.052	3.326	−3.049	0.577	±0.575
EGM2008	0.048	3.831	−2.882	0.603	±0.602

Table 3
Validation of the GOSG01S, GOTIM05S, GODIR05S, GOTIM04S, GODIR04S, GOSPW04S, GOCO03S, JYY_GOCE02S, and EGM2008 models up to degree and order 200 using GPS-leveling data in USA (6169 points) (unit: m). The omission errors were disregarded.

Model	Mean	Max	Min	RMS	STD
GOSG01S	−0.567	2.253	−3.039	0.766	±0.516
GOTIM05S	−0.567	2.243	−3.056	0.765	±0.513
GODIR05S	−0.569	2.243	−3.059	0.767	±0.514
GOTIM04S	−0.563	2.225	−3.060	0.762	±0.513
GODIR04S	−0.567	2.215	−3.080	0.765	±0.514
GOSPW04S	−0.568	2.271	−3.053	0.767	±0.516
GOCO03S	−0.566	2.287	−3.099	0.768	±0.519
JYY_GOCE02S	−0.571	2.220	−3.027	0.769	±0.515
EIGEN-6C2	−0.567	2.267	−3.040	0.767	±0.517
EGM2008	−0.567	2.277	−3.046	0.766	±0.516

Table 4
Validation of the GOSG01S, GOTIM05S, GODIR05S, GOTIM04S, GODIR04S, GOCO03S, JYY_GOCE02S, and EGM2008 models using GPS-leveling data in China and USA (unit: m). The omission errors were compensated using the EGM2008 coefficients up to degree/order 2190.

Model	Degree	Mean (China)	STD (China)	Mean (USA)	STD (USA)
GOSG01S	200	0.242	±0.165	−0.511	±0.283
GOTIM05S	200	0.239	±0.161	−0.511	±0.281
GODIR05S	200	0.240	±0.161	−0.513	±0.281
GOTIM04S	200	0.241	±0.161	−0.507	±0.280
GODIR04S	200	0.239	±0.162	−0.511	±0.281
GOSPW04S	200	0.235	±0.163	−0.512	±0.283
GOCO03S	200	0.238	±0.164	−0.511	±0.285
JYY_GOCE02S	200	0.245	±0.160	−0.517	±0.282
EIGEN-6C2	1949	0.243	±0.167	−0.511	±0.284
EGM2008	200	0.239	±0.240	−0.511	±0.284

16 cm in China show that GOCE has improved the accuracy of the global models beyond degree 90 considering that EGM2008 is used as the background model for reducing omission errors. The reason should be that the accuracy of the data used for the determination of the EGM2008 model is poor in China. From the figure, although the GOSG01S model show slightly better performance than other models with the truncation degree less than 160 in USA, the differences of STD geoid height differences among all the models are less than 5 mm for the truncation degree less than or equal to 200. GOSG01S and GOSPW04S have worse performance for degrees greater than 200 than other models.

The geoid height/height anomaly slope differences are also used to validate the models in our study, which are more sensitive to mid- to high-frequency variations of the geoid [64]. For the definition of the geoid height/height anomaly slope differences, we refer to the Ref. [64]. Fig. 7 shows the RMS of geoid slope differences per distance class for China and USA for the GOCE related models and the EGM2008 model with the truncated degree 200 (in Fig. 7a and b). Here the distance class is selected by the step of 20 km. In order to find the differences between the curves, we choose the RMS of GOSG01S as the reference, which is subtracted from all RMSs of geoid slope differences per distance class (in Fig. 7c and d). In order to get the positive RMS, all RMSs are added by 10 cm. From the figure, the RMSs of slope differences from the GOCE-based models are very close to each other in China when the distance is less than 4800 km, which is same situation in USA. And EGM2008 also shows very poor performance comparing with the other models in China, while all models have a similar performance in USA. This is consistent with the validation results by height anomaly/geoid height differences.

5. Summary and concluding remarks

We derived the new GOCE-only satellite model GOSG01S with a spectral resolution complete to degree/order 220 based on applying the point-wise acceleration approach to process 8 months of the PKI orbits, while a least-squares analysis with the band-pass ARMA filter was used to process 20.5 months of the SGG data. The VCE technique was further applied to estimate the variance factors for every arc of continuous observations (V_{xx}, V_{yy}, V_{zz}) and the variance factors of the independent SST arcs iteratively. A relative weight between the SGG and SST data was set equal to 1. The second-order Tikhonov regularization technique was applied to the near-zonal coefficients ($m < 20$) in order to solve the ill-posed problem caused by the inclination of 96.7° of the GOCE satellite orbit. And GCV method is used to estimate the optimal regularization parameter.

The validation of GOSG01S revealed a similar accuracy with available models. The comparison of the spectral properties of GOSG01S with GOTIM04S, GODIR04S, GOSPW04S and JYY_GOCE02S in terms of the degree RMS of the differences relative to the ultra-high degree model EIGEN-6C2 showed that if we took no account of the lower-order terms, the GOCE-related models except GODIR04S are very close to each other at the spectral window approximately between 80 and 190 due to the same period SGG data used to compile these models. Further validation using GPS-leveling data in China and USA revealed that GOSG01S, GOTIM05S, GODIR05S, GOTIM04S, GODIR04S, GOSPW04S and JYY_GOCE02S have a very similar accuracy, while a low accuracy of EGM2008 at GPS-leveling data in China is caused by the fact that terrestrial gravity data were not used for processing this model. The statistical analysis further showed that the STD of the geoid/quasigeoid differences of GOSG01S (up to degree/order 200) at GPS-leveling points in China and USA is ±57.0 and ±51.5 cm respectively (when disregarding the omission errors), while the corresponding STD of these differences is only ±16.5 and ±28.2 cm (when taking the omission errors into consideration). Moreover, in agreement with previous findings, we demonstrated that GOSG01S comprises more information on gravity field that EGM2008 in areas with a lack or total absence of terrestrial gravity data. These results

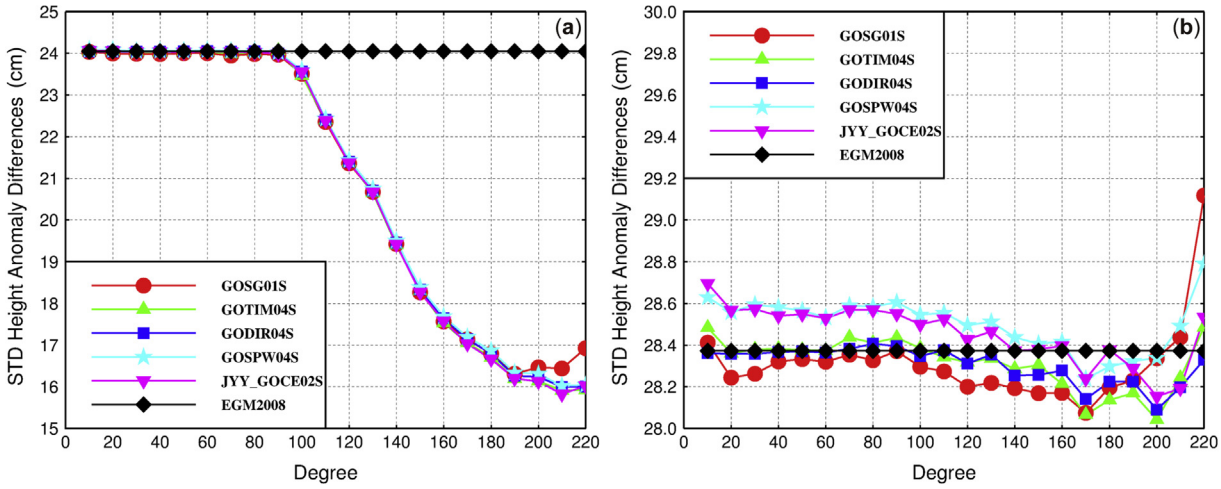

Fig. 6. STDs of (**a**) height anomaly differences in China and (**b**) geoid height differences in USA for the selected truncation degrees for the GOCE related models and the EGM2008 model. Red GOSG01S, green GOTIM04S, blue GODIR04S, cyan GOSPW04S, magenta JYY_GOCE02S, black EGM2008.

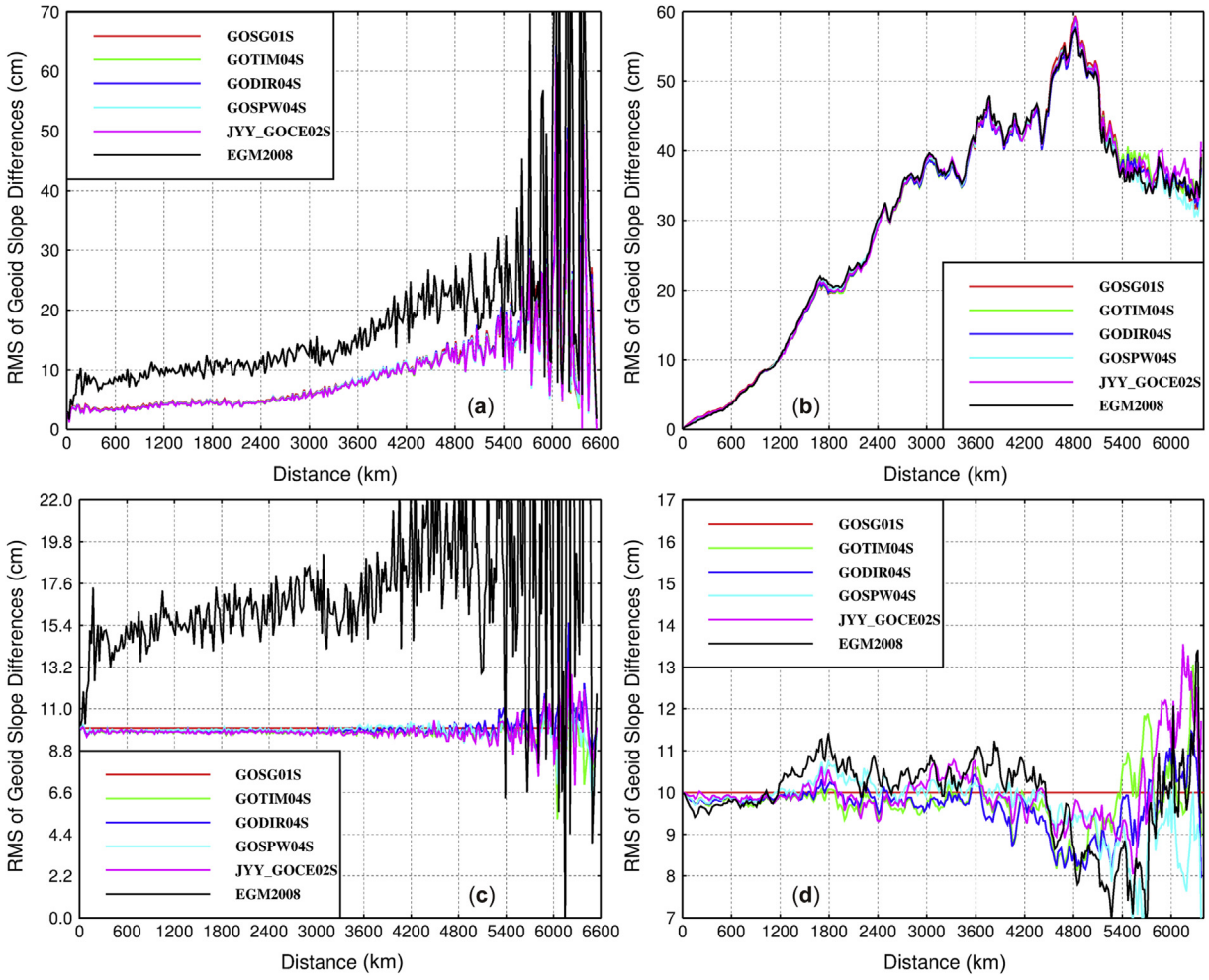

Fig. 7. RMS of geoid slope differences per distance class for China (**a, c**) and USA (**b, d**) for the GOCE related models and the EGM2008 model up to the degree and order 200. Red GOSG01S, green GOTIM04S, blue GODIR04S, cyan GOSPW04S, magenta JYY_GOCE02S, black EGM2008. In the bottom panels, the RMS of GOSG01S is subtracted from all RMSs of geoid slope differences per distance class, and all RMSs except the one of GOSG01S are added by 10 cm.

confirmed a good performance of processing strategies applied in this study to compile our GOCE-only satellite model GOSG01S.

Author contributions

X.X.,Y.Z. and T.R.conceived, designed and performed the data processing; X.X. wrote the paper; R.T. reviewed the manuscript.

Acknowledgments

This research was financially supported by the National Key Basic Research Program of China (973 program, grant no.: 2013CB733302, 2013CB733301), the Major International (Regional) Joint Research Project (grant no.: 41210006), DAAD Thematic Network Project (grant no.: 57173947), and the National Natural Science Foundation of China (grant No. 41374022). The authors acknowledge the European Space Agency for providing the GOCE data.

Appendix

The GOCE only model GOSG01S will be provided as an appendix of the paper. The brief description of the data used and progress strategies about the model are described as follows.

Description of data used

- Period:
  - SGG: 1/11/2009–31/5/2012
  - SST: 1/11/2009–5/7/2010
- Sampling interval: 1s
- SGG: EGG_NOM_2 (GGT: Vxx, Vyy, Vzz) in GRF
- SST: SST_PKI_2, SST_PCV_2, SST_PRD_2
- Attitude: EGG_NOM_2 (IAQ), SST_PRM_2 (PRM)
- Non-conservative force: Common mode ACC (GG_CCD_1i)
- Background model: tidal model (solid etc.), third-body acceleration, relativistic corrections, …

Data progress strategies

- Data preprocessing
  - Gross outlier elimination and interpolation (only for the data gaps less than 40s).
  - Splitting data into subsections for gaps >40s
- The normal equation from SST data
  - Point-wise acceleration approach (PAA)
  - Extended Differentiation Filter (low-pass)
  - Max degree: up to 130
  - Data: PKI, PCV, CCD
- The normal equation from SGG data

- Space-Wise LS method
- Max degree: up to 220
- Data:GGT, PRD, IAQ, PRM
- Band-pass filter: used to deal with colored-noise of GGT observations (pass band 0.005–0.041 Hz)
- Forming the normal equations according to subsections
- Spherical harmonic base function transformation instead of transforming GGT from GRF to LNRF

➢ Combination of SGG and SST
- Max degree: up to 220
- The VCE technique is used to estimate the relative weights forV_{xx}, V_{yy}, V_{zz}
- Tikhonov Regularization Technique (TRT) is only applied to near (zonal) terms (m < 20)
- Strictly inverse the normal matrix based on MPI

➢ Parameters for the model recovery
- Earth_gravity_constant: 3.986004415E+14
- Radius: 6.3781363E+06
- Max_degree: 220
- Tide_system: tide_free

References

[1] ESA, Gravity Field and Steady-State Ocean Circulation Mission. Report for mission selection; the four candidate earth explorer missions, ESA SP-1233(1), ESA Publications Division, Noordwijk, Netherlands, 1999.
[2] R. Rummel, G. Balmino, J. Johannessen, P. Visser, P. Woodworth, Dedicated gravity field missions: principles and aims, J. Geodyn. 33 (2002) 3–20.
[3] M.R. Drinkwater, R. Floberghagen, R. Haagmans, D. Muzi, A. Popescu, GOCE: ESA's first Earth Explorer Core mission, in: G.B. Beutler, M. Drinkwater, R. Rummel, R. von Steiger (Eds.), Earth Gravity Field from Space – from Sensors to Earth Sciences, vol. 18, Kluwer Academic Publishers, Dordrecht, Netherlands, 2003, pp. 419–432.
[4] C. Stummer, T. Fecher, R. Pail, Alternative method for angular rate determination within the GOCE gradiometer processing, J. Geod. 85 (2011) 585–596.
[5] H. Bock, A. Jäggi, U. Meyer, P. Visser, J. van den Ijssel, T. van Helleputte, et al., GPS-derived orbits for the GOCE satellite, J. Geod. 85 (2011) 807–818.
[6] R. Pail, H. Goiginger, R. Mayrhofer, W.D. Schuh, J.M. Brockmann, I. Krasbutter, et al., GOCE gravity field model derived from orbit and gradiometry data applying the time-wise method, in: H. Lacoste-Francis (Ed.), Proceedings of the ESA Living Planet Symposium, Bergen, Norway, 28 June–2 July 2010, ESA Communications, Bergen, Norway, 2010.
[7] J.M. Brockmann, N. Zehentner, E. Höck, R. Pail, I. Loth, T. Mayer-Gürr, et al., EGM_TIM_RL05: an independent geoid with centimeter accuracy purely based on the GOCE mission, Geophys. Res. Lett. 41 (2014) 8089–8099.
[8] S.L. Bruinsma, C. Förste, O. Abrikosov, J.M. Lemoine, J.C. Marty, S. Mulet, et al., ESA's satellite-only gravity field model via the direct approach based on all GOCE data, Geophys. Res. Lett. 41 (2014) 7508–7514.
[9] R. Pail, S. Bruinsma, F. Migliaccio, C. Förste, H. Goiginger, W.D. Schuh, et al., First GOCE gravity field models derived by three different approaches, J. Geod. 85 (2011) 819–843.
[10] M. Schneider, A General Method of Orbit Determination, Royal Aircraft Translation, Number 1279, Ministry of Technology, Farnborough, UK, 1968.
[11] T. Mayer-Gürr, K.H. Ilk, A. Eicker, M. Feuchtinger, ITG-CHAMP01: a CHAMP gravity field model from short kinematic arcs over a one-year observation period, J. Geod. 78 (2005) 462–480.
[12] T. Mayer-Gürr, A. Eicker, K.H. Ilk, Gravity field recovery from GRACE-SST data of short arcs, in: J. Flury, R. Rummel, C. Reigber, M. Rothacher, G. Boedeker, U. Schreiber (Eds.), Observation of the Earth System from Space, Springer, Berlin, Germany, 2006, pp. 131–148.
[13] S.L. Bruinsma, J.C. Marty, G. Balmino, R. Biancale, C. Förste, O. Abrikosov, et al., GOCE gravity field recovery by means of the direct numerical method, in: H. Lacoste-Francis (Ed.), Proceedings of the ESA Living Planet Symposium, Bergen, Norway, 28 June–2 July 2010, ESA Communications, Bergen, Norway, 2010.
[14] S.L. Bruinsma, J.M. Lemoine, R. Biancale, N. Vales, CNES/GRGS 10-day gravity field models (release 2) and their evaluation, Adv. Space Res. 45 (2010) 587–601.
[15] B. Metzler, R. Pail, GOCE data processing: the spherical cap regularization approach, Stud. Geophys. Geod. 49 (2005) 441–462.
[16] C. Dahle, F. Flechtner, C. Gruber, D. König, R. König, G. Michalak, et al., GFZ GRACE Level-2 Processing Standards Document for Level-2 Product Release 0005, (Scientific Technical Report – Data, 12/02), Potsdam, Germany, 2012.
[17] A. Gatti, M. Reguzzoni, F. Migliaccio, F. Sanso, Space-wise grids of gravity gradients from GOCE data at nominal satellite altitude, in: In the 5th GOCE User Workshop, Paris, France, 25–28 November 2014.
[18] F. Migliaccio, M. Reguzzoni, A. Gatti, F. Sanso, M. Herceg, A GOCE-only global gravity field model by the space-wise approach, in: Proceedings of 4th International GOCE User Workshop, 2011. Munich, Germany.
[19] M. Reguzzoni, N. Tselfes, Optimal multi-step collocation: application to the space-wise approach for GOCE data analysis, J. Geod. 83 (2009) 13–29.
[20] J. Schall, A. Eicker, J. Kusche, The ITG-Goce02 gravity field model from GOCE orbit and gradiometer data based on the short arc approach, J. Geod. 88 (2014) 403–409.
[21] W. Yi, An alternative computation of a gravity field model from GOCE, Adv. Space Res. 50 (2012) 371–384.
[22] H. Hashemi Farahani, P. Ditmar, R. Klees, X. Liu, Q. Zhao, J. Guo, The static gravity field model DGM-1S from GRACE and GOCE data: computation, validation and an analysis of GOCE mission's added value, J. Geod. 87 (2013) 843–867.
[23] T. Mayer-Gürr, A. Kvas, B. Klinger, D. Rieser, N. Zehentner, R. Pail, et al., The combined satellite gravity field model GOCO05s, in: EGU 2015, Vienna, Austria, April 2015.
[24] R. Rummel, Satellite gradiometry, in: H. Sünkel (Ed.), Mathematical and Numerical Techniques in Physical Geodesy, vol. 7, Springer, Berlin, Germany, 1986, pp. 317–363. Lecture Notes in Earth Sciences.
[25] O. Baur, N. Sneeuw, E.W. Grafarend, Methodology and use of tensor invariants for satellite gravity gradiometry, J. Geod. 82 (2007) 279–293.
[26] J.H. Yu, X.Y. Wan, Recovery of the gravity field from GOCE data by using the invariants of gradient tensor, Sci. China Earth Sci. 56 (2012) 1193–1199.
[27] N. Sneeuw, A Semi-analytical Approach to Gravity Field Analysis from Satellite Observations, PhD thesis, Institut für Astronomische und Physikalische Geodäsie, Technische Universität München, Munich, Germany, 2000.
[28] R. Pail, B. Metzler, T. Preimesberger, B. Lackner, M. Wermuth, GOCE quick-look gravity field analysis in the framework of HPF, in: Proceedings of 3rd GOCE User Workshop, Frascati, ESRIN, November 2006, European Space Agency, Noordwijk, Netherlands, 2007, pp. 325–332.
[29] R. Mayrhofer, R. Pail, T. Fecher, Quick-look gravity field solutions as part of the GOCE quality assessment, in: H. Lacoste-Francis (Ed.), Proceedings of the ESA Living Planet Symposium, Bergen, Norway, 28 June–2 July 2010, ESA Communications, Bergen, Norway, 2010.
[30] C. Jekeli, The determination of gravitational potential differences from satellite-to-satellite tracking, Celest. Mech. Dyn. Astr. 75 (1999) 85–101.
[31] P. Ditmar, A. van Eck van der Sluijs, A technique for modeling the Earth's gravity field on the basis of satellite accelerations, J. Geod. 78 (2004) 12–33.
[32] L. Prange, A. Jäggi, G. Beutler, L. Mervart, R. Dach, Gravity field determination at the AIUB–the celestial mechanics approach, in: Observing Our Changing Earth, Proceedings of the 2007 IAG General Assembly, Perugia, Italy, 2–13 July 2007, Springer, Berlin, Germany, 2009, pp. 353–362.
[33] T. Reubelt, G. Austen, E.W. Grafarend, Harmonic analysis of the Earth's gravitational field by means of semi-continuous ephemerides of a low Earth orbiting GPS-tracked satellite. Case study: CHAMP, J. Geod. 77 (2003) 257–278.
[34] O. Baur, H. Bock, E. Höck, A. Jäggi, S. Krauss, T. Mayer-Gürr, et al., Comparison of GOCE-GPS gravity fields derived by different approaches, J. Geod. 88 (2014) 959–973.
[35] W.A. Heiskanen, H. Moritz, Physical Geodesy, W.H. Freeman & Company, San Francisco, USA, 1967.
[36] R. Koop, Global Gravity Field Modeling Using Satellite Gravity Gradiometry, Publications on Geodesy, New Series, Number 38, Netherlands Geodetic Commission, Delft, Netherlands, 1993.
[37] S. Cesare, Performance Requirements and Budgets for the Gradiometric Mission. GO-TN-AI-0027, Issue 4, Turin, Italy, 2008.
[38] T. Reubelt, M. Götzelmann, E.W. Grafarend, Harmonic analysis of the Earth's gravitational field from kinematic CHAMP orbits based on numerically derived satellite accelerations, in: J. Flury, R. Rummel, C. Reigber, M. Rothacher, G. Boedeker, U. Schreiber (Eds.), Observation of the Earth System from Space, Springer, Berlin, Germany, 2006, pp. 27–42.
[39] M. Götzelmann, W. Keller, T. Reubelt, Gross error compensation for gravity field analysis based on kinematic orbit data, J. Geod. 80 (2006) 184–198, http://dx.doi.org/10.1007/s00190-006-0061-9.
[40] T. Reubelt, Harmonische Gravitationsfeldanalyse aus GPS-vermessenen kinematischen Bahnen niedrig fliegender Satelliten vom Typ CHAMP, GRACE und GOCE mit einem hoch auflösenden Beschleunigungsansatz, Deutsche Geodätische Kommission, C 632, Verlag der Bayerischen Akademie der Wissenschaften, Munich, Germany, 2009.
[41] O. Baur, T. Reubelt, M. Weigelt, M. Roth, N. Sneeuw, GOCE orbit analysis: long-wavelength gravity field determination using the acceleration approach, Adv. Space Res. 50 (2012) 385–396.
[42] T. Reubelt, O. Baur, M. Weigelt, M. Roth, N. Sneeuw, GOCE long-wavelength gravity field recovery from 1s-sampled kinematic orbits using the acceleration approach, in: U. Marti (Ed.), Gravity, Geoid and Height Systems, Proceedings of the IAG symposium GGHS2012, Venice, Italy, 9–12 October 2012, Springer, 2014, pp. 21–26.
[43] M. Weigelt, T. Van Dam, A. Jäggi, L. Prange, M.J. Tourian, W. Keller, et al., Time-variable gravity signal in Greenland revealed by high-low satellite-to-satellite tracking, J. Geophys. Res. Solid Earth 118 (2012) 3848–3859.
[44] EGG-C, GOCE Level 2 Product Data Handbook. GO-MA-HPF-GS-0110, Issue 4.3, 2010.
[45] K.R. Koch, J. Kusche, Regularization of geopotential determination from satellite data by variance components, J. Geod. 76 (2002) 259–268.

[46] F.R. Helmert, Die Ausgleichungsrechnung nach der Methode der kleinsten Quadrate, 3rd ed., Teubner, Leipzig, 1924.
[47] A.N. Tikhonov, Regularization of ill-posed problem, Dokl. Akad. Nauk SSSR 151 (1963) 49–52.
[48] J. Kusche, R. Klees, Regularization of the gravity field estimation from satellite gravity gradients, J. Geod. 76 (2002) 359–368.
[49] P. Ditmar, J. Kusche, R. Klees, Computation of spherical harmonic coefficients from gravity gradiometry data to be acquired by the GOCE satellite: regularization issues, J. Geod. 77 (2003) 465–477.
[50] W.M. Kaula, Theory of Satellite Geodesy, Blaisdell Publishing Company, Waltham Massachusetts, USA, 1966.
[51] A. Jäggi, H. Bock, U. Meyer, G. Beutler, J. van den Ijssel, GOCE: assessment of GPS-only gravity field determination, J. Geod. 89 (2015) 33–48.
[52] W.D. Schuh, Improved modelling of SGG-data sets by advanced filter strategies, in: ESA-Project "From Eötvös to mGal+". Final report, ESA/ESTEC Contract 14287/00/NL/DC, WP 2. ESA, Noordwijk, Netherlands, 2002, pp. 113–181.
[53] L.H. Zhang, B.Y. Zheng, Stochastic Signal Processing (in Chinese), Tsinghua University Press, Beijing, China, 2003.
[54] F.G. Lemoine, S.C. Kenyon, J.K. Factor, R.G. Trimmer, N.K. Pavlis, D.S. Chinn, et al., The Development of the Joint NASA GSFC and NIMA Geopotential Model EGM96. NASA/TP-1998-206861, NASA Goddard Space Flight Center, Greenbelt, Maryland, USA, 1998.
[55] M.J. Fuchs, J. Bouman, Rotation of GOCE gravity gradients to local frames, Geophys. J. Int. 187 (2011) 743–753.
[56] A. Jäggi, L. Prange, U. Hugentobler, Impact of covariance information of kinematic positions on orbit reconstruction and gravity field recovery, Adv. Space Res. 47 (2011) 1472–1479.
[57] A. Jäggi, H. Bock, L. Prange, U. Meyer, G. Beutler, GPS-only gravity field recovery with GOCE, CHAMP, and GRACE, Adv. Space Res. 47 (2011) 1020–1028.
[58] R. Rummel, W. Yi, C. Stummer, GOCE gravitational gradiometry, J. Geod. 85 (2011) 777–790.
[59] N. Sneeuw, M. van Gelderen, The polar gap, in: F. Sansò, R. Rummel (Eds.), Geodetic Boundary Value Problems in View of the One Centimeter Geoid, vol. 65, Springer, 1997, pp. 559–568. Lecture Notes in Earth Sciences.
[60] C. Förste, S. Bruinsma, F. Flechtner, J.C. Marty, J.M. Lemoine, C. Dahle, et al., A preliminary update of the direct approach GOCE processing and a new release of EIGEN-6C, in: AGU Fall Meeting, San Francisco, USA, 3–7 December 2012.
[61] J.C. Li, W.P. Jiang, X.C. Zou, X.Y. Xu, W.B. Shen, Evaluation of recent GRACE and GOCE satellite gravity models and combined models using GPS/leveling and gravity data in China, in: U. Marti (Ed.), Gravity, Geoid and Height Systems, Proceedings of the IAG symposium GGHS2012, Venice, Italy, 9–12 October 2012, Springer, 2014, pp. 67–74.
[62] N.K. Pavlis, S.A. Holmes, S.C. Kenyon, J.K. Factor, The development and evaluation of the Earth gravitational model 2008 (EGM2008), J. Geophys. Res. Solid Earth 117 (2012) 1978–2012.
[63] D.G. Milbert, Documentation for the GPS Benchmark Data Set of 23-July-98, IGeS Bulletin N. 8, International Geoid Service, Milan, 1998, pp. 29–42.
[64] T. Gruber, P. Visser, C. Ackermann, M. Hosse, Validation of GOCE gravity field models by means of orbit residuals and geoid comparisons, J. Geod. 85 (2011) 845–860.

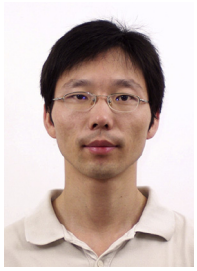

Xinyu Xu (Associate Professor). Education and degrees: 1) Ph.D., School of Geodesy and Geomatics, Wuhan University, Wuhan, 2008, 2) M.S., School of Geodesy and Geomatics, Wuhan University, Wuhan, 2004, 3) B.S., School of Geodesy and Geomatics, Wuhan University, Wuhan, 2001. Academic positions: 1) 2008–2011, Lecturer, School of Geodesy and Geomatics, Wuhan University, 2) 2009–2010, Visiting Scholar, Institute of Geodesy, Universität Stuttgart. 3) 2012-present, Associate Professor, School of Geodesy and Geomatics, Wuhan University. Research Interests: 1) Satellite geodesy and physical geodesy. 2) The Determination of Global Gravity Field Model from Satellite Gravity Data and its applications.